Journal of Magnetism and Magnetic Materials 479 (2019) 312–316

Contents lists available at ScienceDirect

Journal of Magnetism and Magnetic Materials

journal homepage: www.elsevier.com/locate/jmmm

Research articles

Element selective magnetism in $Ho_{0.5}Nd_{0.5}Fe_3(BO_3)_4$ single crystal probed with hard X-ray magnetic circular dichroism

Mikhail Platunov[a,b,*], Natalia Kazak[a], Viacheslav Dudnikov[a], Vladislav Temerov[a], Irina Gudim[a], Yurii Knyazev[a], Sergey Gavrilkin[d], Vadim Dyadkin[c], Iurii Dovgaliuk[c], Dmitry Chernyshov[c], Amir Hen[b], Fabrice Wilhelm[b], Andrei Rogalev[b], Sergei Ovchinnikov[a]

[a] Kirensky Institute of Physics, Federal Research Center KSC SB RAS, Akademgorodok 50, bld. 38, 660036 Krasnoyarsk, Russia
[b] ESRF-The European Synchrotron, 71 Avenue des Martyrs CS40220, F-38043 Grenoble Cedex 9, France
[c] Swiss-Norwegian Beamlines at the ESRF, 71 Avenue des Martyrs CS40220, F-38043 Grenoble Cedex 9, France
[d] P.N. Lebedev Physical Institute of RAS, 119991 Moscow, Russia

ARTICLE INFO

Keywords:
X-ray magnetic circular dichroism
X-ray absorption
Magnetic properties

ABSTRACT

We present a study of a $Ho_{0.5}Nd_{0.5}Fe_3(BO_3)_4$ single crystal aiming at understanding the roles of each magnetic sublattices in magnetic transitions at low temperatures. The crystal structure is determined to have the *R*32 symmetry in whole studied temperature range but the crystal appears to be racemic. Element selective magnetic properties studied with X-ray magnetic circular dichroism at the $L_{2,3}$-edges of Ho and Nd, and at the Fe *K*-edge at $T = 3$ K under magnetic fields of ± 17 T are compared with the results of macroscopic magnetization measurements in pure and substituted crystals. All three magnetic sublattices are shown to be strongly coupled and to undergo a spin-reorientation transition when magnetic field is applied along the trigonal *c*-axis. On the contrary, when magnetic field is applied in the *ab*-plane only the holmium atoms exhibit a sizeable magnetization jump. This result allows us to conclude that the spin-flop transitions observed in macroscopic magnetization curves and associated anomalies of electric polarization are due to the Ho^{3+} magnetic moment reorientation.

1. Introduction

Rare-earth ferroborates $REFe_3(BO_3)_4$ belong to a very intriguing class of materials that exhibit simultaneously magnetic and electric polarization order, *i.e.* these crystals are multiferroic. They have been extensively studied since 1970s mainly due to their large magnetoelectric susceptibility [1–11], a strong nonlinear optical response [12,13] and large optical activity in wide spectral range from x-rays [14,15] to gigahertz [10,16].

Rare-earth ferrobotaes crystallize in the noncentrosymmetrical trigonal *R*32 or $P3_121$ space groups [17] depending on the rare-earth ion radius. Light rare-earth ions from La to Sm favor the *R*32 crystal structure down to very low temperatures whereas in compounds with Y and heavier rare-earth ions from Eu to Yb, decreasing the temperature systematically leads to a first-order structural phase transition from *R*32 to $P3_121$ structure [18,19]. For example, pure $HoFe_3(BO_3)_4$ undergoes a structural phase transition at 430 K [19] from the space group *R*32 to the group $P3_121$, while the structure of pure $NdFe_3(BO_3)_4$ crystal remains *R*32 at all temperatures. An interesting structural feature common to both structures is the presence of chiral chains formed by edge-shared FeO_6 octahedra, which are propagated along the trigonal *c*-axis. The distance between Fe^{3+} ions ($d_{Fe-Fe} \sim 3.2$ Å) along these chains is significantly shorter than the distance between neighbouring chains ($d_{Fe-Fe} \sim 4.83$ Å) and this leads to a strong anisotropy of various properties in these crystals. In the unit cell of *R*32 structure (the $NdFe_3(BO_3)_4$ structure shown on Fig. 1, as an example) there are three such chains which are interconnected by REO_6 triangular prisms (the inter-ionic distance $d_{RE-RE} \sim 6$ Å), and by equilateral triangles of BO_3 forming a unified three-dimensional structure.

In all rare-earth ferroborates the iron sublattice is ordered antiferromagnetically at low temperatures, typically below $T_N = 30$–40 K. Given the fact that the antiferromagnetic transition temperature is nearly independent of rare-earth ion, it is generally assumed that the rare-earth sublattice is not ordered and is very weakly coupled to the iron sublattice. This picture is also supported by an apparent paramagnetic behavior, eventhough strongly anisotropic, of magnetization curves, down to the lowest temperatures. Strikingly, the direction of Fe^{3+} pure spin moments of $\approx 5\ \mu_B$ in the ordered state is determined by

* Corresponding author.
E-mail address: platunov@iph.krasn.ru (M. Platunov).

https://doi.org/10.1016/j.jmmm.2019.02.040
Received 26 November 2018; Accepted 14 February 2019
Available online 14 February 2019
0304-8853/

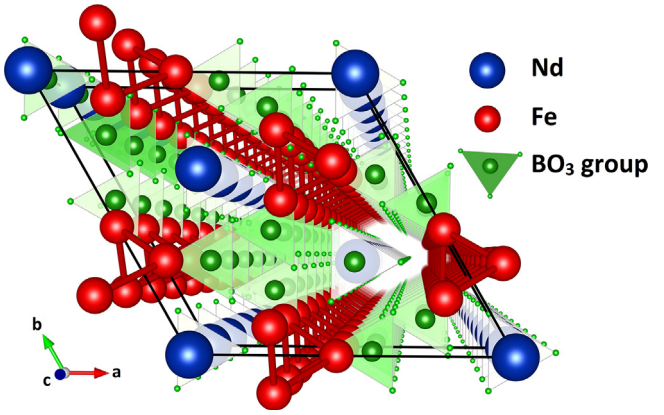

Fig. 1. (a) Crystal structure of $NdFe_3(BO_3)_4$ crystal. The material can be described using the rhombohedral space group *R*32. Fe (red) is coordinated by oxygen octahedra, which form edge sharing helical chains along the trigonal *c*-axis. These chains and Nd (blue) atoms are connected in the *ab*-plane by BO_3 groups (green). (For interpretation of the references to colour in this figure legend, the reader is referred to the web version of this article.)

the local anisotropy of the RE^{3+} ions. For instance, in the case of a $NdFe_3(BO_3)_4$ crystal the magnetic moments of both Fe^{3+} and Nd^{3+} were shown to lie in the basal *ab*-plane below $T_N = 31$ K [1] and are antiferromagnetically oriented with some non-collinearity. The angle between Nd and Fe moments was found to be temperature dependent [20]. The magnetic moments of Ho^{3+} and Fe^{3+} in $HoFe_3(BO_3)_4$ are also lying in the basal plane below $T_N = 38$ K [21]. However, a competition of an easy-axis anisotropy of Ho^{3+} ions and exchange in-plane anisotropy of the Fe sublattice leads to the spontaneous spin-reorientation transition to an easy-axis antiferromagnetic structure below $T_{SR} = 5$ K [21]. Furthermore, both $HoFe_3(BO_3)_4$ and $NdFe_3(BO_3)_4$ systems show an external field-induced spin-flop and spin-reorientation transitions, that are associated with reorientation of the magnetic moments of Fe and *RE* sublattices. In the $NdFe_3(BO_3)_4$, magnetization curves are practically linear and independent of temperature when a magnetic field is applied along the *c*-axis as expected for a crystal with an easy-plane anisotropy. However, when a magnetic field applied in the *ab*-plane, the spin-flop transition is observed at $H_{SF} \approx 0.7$ T [22]. In the case of $HoFe_3(BO_3)_4$ magnetization curves are strongly non-linear and the spin-flop transitions are very pronounced for both directions of magnetic field: at $H_{SF} \approx 0.6$ T when magnetic field is applied along the trigonal *c*-axis and at $H_{SF} \approx 1$ T for a magnetic field applied in the *ab*-plane [23] (data of the present study are shown on Fig. 2). Magneto-electric properties of these two crystals are also very different. A $HoFe_3(BO_3)_4$ crystal exhibits a zero-field spontaneous electrical polarization of $\sim 90\ \mu C/m^2$ along the *c*-axis below T_N, which was shown to decrease when an external magnetic field is applied [21]. A $NdFe_3(BO_3)_4$ crystal shows in turn the electric polarization as large as 300 $\mu C/m^2$ in *ab*-plane, which is strongly affected by an applied magnetic field and the compound exhibits a giant quadratic magnetoelectric effect [1,24].

In this study, we focused on the $Ho_{0.5}Nd_{0.5}Fe_3(BO_3)_4$ single crystal, which is distinguished by its magnetic and magnetoelectric properties from the pure $HoFe_3(BO_3)_4$ and $NdFe_3(BO_3)_4$ compounds. The substitution of 50% Ho^{3+} ions with Nd^{3+} ions leads to the stabilization of an easy-axis phase below $T_N = 32$ K and leads to an increase of the temperature of spontaneous spin-reorientation transition to $T_{SR} = 9$ K [21]. Also, the field-induced spin-reorientation (spin-flop) transitions observed in the parent compounds are shifted to the high-field regions: from ~ 0.6 T to 1 T for field applied along the *c*-axis and from ~ 0.9 T to 2.3 T for magnetic field applied in the *ab*-plane (Fig. 2). Most interestingly, the solid solution of $Ho_{0.5}Nd_{0.5}Fe_3(BO_3)_4$ combines the main features observed in the two end members: the zero-field spontaneous electric polarization, which diminishes under magnetic fields along the

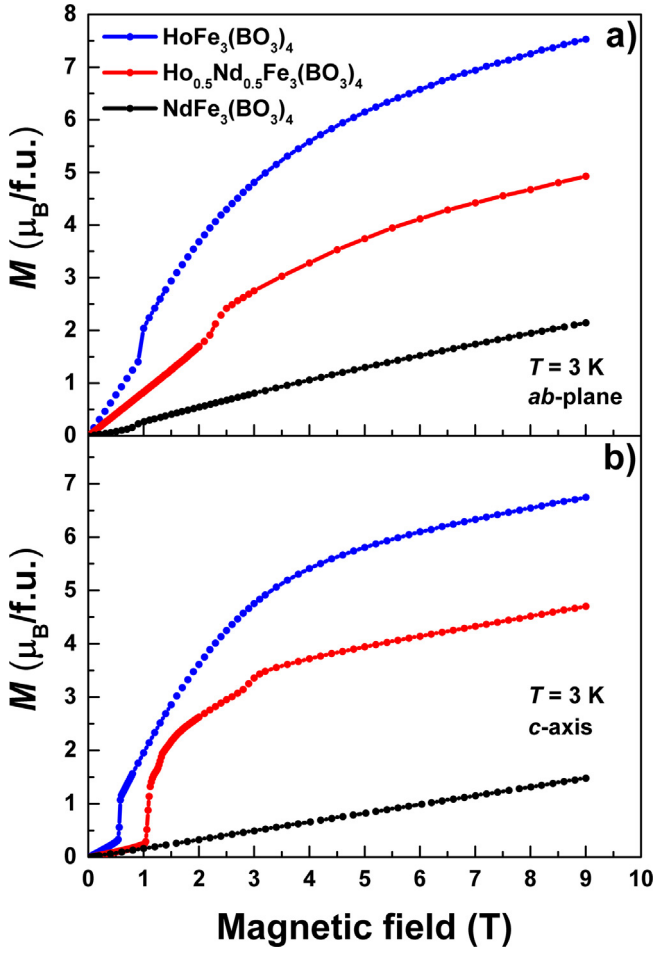

Fig. 2. (a) Field dependences of the magnetizations for $Ho_{1-x}Nd_xFe_3(BO_3)_4$ ($x = 0.0, 0.5, 1.0$) for the applied magnetic field in the basal *ab*-plane (a) and the trigonal *c*-axis (b), $T = 3$ K.

c-axis in a similar manner as for $HoFe_3(BO_3)_4$; and a large value of electric polarization (up to 900 $\mu C/m^2$ at 7 T) induced by the magnetic fields along the *a*-axis exceeding by a factor of 2 that of $NdFe_3(BO_3)_4$. Thus, the $Ho_{0.5}Nd_{0.5}Fe_3(BO_3)_4$ demonstrates a complex behavior in both temperature and field dependencies of the electric polarization, which is correlated with the spin-flop features observed in the magnetization curves [21]. Hence, the 50% neodymium substitution causes two different but related effects: the enhancement of the easy-axis magnetic anisotropy and an increase in the spontaneous polarization. This suggests that the magnetic and magneto-electric properties of a $Ho_{0.5}Nd_{0.5}Fe_3(BO_3)_4$ cannot be described by a simple combination of contributions on the parent crystals. Indeed, magnetic and electronic degrees of freedom in this complex crystal are strongly interrelated and mutually coupled. A lattice degree of freedom could also play a role since the parent compounds have similar but different crystal structures.

To elucidate a possible relation of this behavior to rare-earth and iron magnetism, a systematic study of an element-specific magnetization has been undertaken using hard X-ray Magnetic Circular Dichroism (XMCD) technique. The results obtained at the *K*-edge of Fe and at the $L_{3,2}$-edges of rare-earth ions allowed us to disentangle the magnetic behavior of Ho, Nd, and Fe sublattices at low temperatures and under an external magnetic field of 17 Tesla. Our study confirms that in a $Ho_{0.5}Nd_{0.5}Fe_3(BO_3)_4$ crystal all three (Ho, Nd and Fe) magnetic sublattices undergo a spin-reorientation transition at $H_{sf}^c = 1$ T when magnetic field is applied along the *c*-axis. This observation unambiguously demonstrates that three sublattices are magnetically

coupled. In the case of magnetic field applied in the *ab*-plane, it is only the holmium sublattice that undergoes the spin-reorientation transition. Therefore, it can be inferred that the Ho^{3+} and Fe^{3+} sublattices are stronger magnetically coupled and that the easy-axis magnetic anisotropy driven by Ho^{3+} ions induces spin-flop transitions in the Fe^{3+} and Nd^{3+} sublattices.

2. Experimental techniques

X-ray diffraction and X-ray absorption spectroscopy experiments have been performed on high quality $Ho_{1-x}Nd_xFe_3(BO_3)_4$ (x = 0.0, 0.5, 1.0) single crystals prepared from the same batch as those described in [21]. Several oriented plates with sizes of several millimeters and of 1 mm thickness were cut from the crystal and optically polished. The crystallographic orientations of the plates were carefully checked using X-ray diffraction. The crystal structure of $Ho_{0.5}Nd_{0.5}Fe_3(BO_3)_4$ in the temperature range 100–300 K was determined using the Pilatus@SNBL diffractometer [25] with the incident beam wavelength set to 0.68239 Å. Macroscopic magnetization measurements of $Ho_{1-x}Nd_xFe_3(BO_3)_4$ (x = 0.0, 0.5, 1.0) single crystals were performed in applied magnetic field up to 9 T (Fig. 2) (parallel and perpendicular to the samples' trigonal *c*-axis) using a commercial Physical Property Measurement System (PPMS) from Quantum Design using the Vibrating Sample Magnetometry (VSM) configuration. Measured curves have been corrected for crystals shape anisotropy.

X-ray Absorption Near-Edge Structure (XANES) and X-ray Magnetic Circular Dichroism (XMCD) measurements have been performed at the Fe *K*- (7112 eV), Ho $L_{3,2}$- (8071, 8919 eV), and Nd $L_{3,2}$- (6208, 6722 eV) absorption edges at the ESRF ID12 beamline [26]. For experiments at the Fe *K*-edge, we have used the fundamental harmonic of Apple-II type (λ_U = 38 mm) helical undulator spectrum. Spectra at the $L_{3,2}$-edges of rare-earth ions were measured with the second harmonic of HELIOS-II (λ_U = 52 mm) helical undulator. In both cases, it was possible to change helicity of emitted x-rays in less than 3 s by translating movable arrays of permanent magnets of the undulators by about 26 mm. To further monochromatize the undulator emission, a fixed-exit double crystal Si (111) monochromator was used at the required photon energies. Samples were mounted on a cold finger of an "amagnetic" He flow cryostat that was inserted in a cold bore of superconducting solenoid with a maximum magnetic field of 17 Tesla. All XANES spectra were recorded using total fluorescence yield detection mode in "back-scattering" geometry using Si photodiodes [27] mounted on liquid nitrogen shield of the solenoid allowing very large solid angle of detection. This detection method has been preferred to the total electron yield since it is insensitive to a magnetic field and probes the bulk properties of the sample. Spectra were measured for two orientations of the crystals: the trigonal *c*-axis parallel (axial) and perpendicular (orthoaxial configuration) with respect to the X-ray wave-vector and an applied magnetic field. The XMCD signal was obtained as differences of XANES spectra measured with opposite helicities of the incoming photons at a fixed magnetic field. Measurements were performed for two directions of applied magnetic field parallel and antiparallel to the incoming X-ray wavevector and that allowed us to ensure the correctness of the final XMCD results. The element-specific magnetization curves were recorded by monitoring the intensity of XMCD signals at respective photon energies as a function of applied magnetic field (± 17 T).

3. Results and discussion

The crystal structure of $Ho_{0.5}Nd_{0.5}Fe_3(BO_3)_4$ was identified to be *R*32 with room temperature lattice parameters: a = b = 9.57280(10) Å, c = 7.58760(10) Å, $\alpha = \beta = 90.00°$, $\gamma = 120.00°$, V = 602.161(15) $Å^3$, and are in good agreement with previous published data [28,29]. No sign of a structural transition in the temperature range 100–300 K was detected. Detailed X-ray structural analysis revealed that the studied

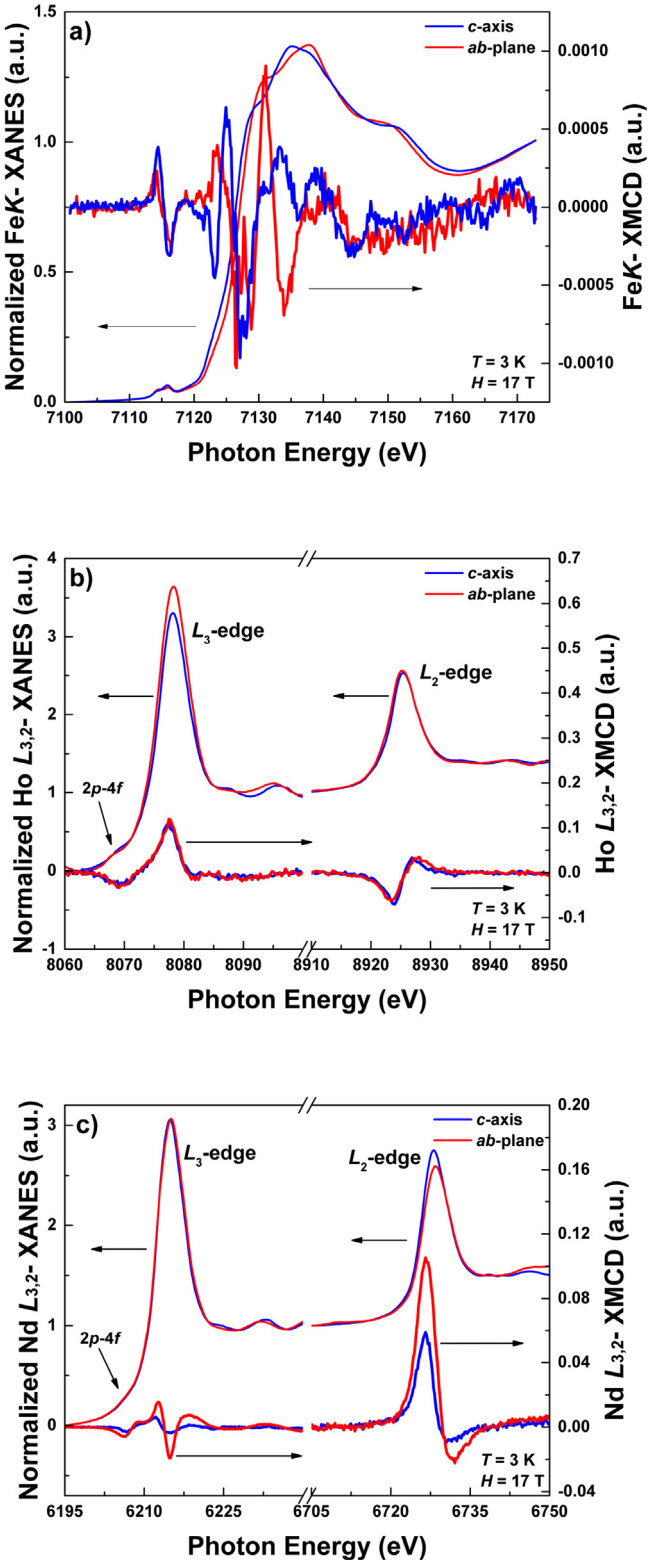

Fig. 3. Normalized XANES/XMCD spectra recorded at 3 K and 17 T for $Ho_{0.5}Nd_{0.5}Fe_3(BO_3)_4$ for different orientations of wave vector k relative to the trigonal *c*-axis: a) Fe *K*-edge; b) Ho $L_{3,2}$-edges; c) Nd $L_{3,2}$-edges.

piece of $Ho_{0.5}Nd_{0.5}Fe_3(BO_3)_4$ single crystal was not enantiopure, *i.e.* a racemic mixture of two twins. The ratio between enantiomeric twin components for racemic $Ho_{0.5}Nd_{0.5}Fe_3(BO_3)_4$ crystal was determined *via* refining the Flack parameter [30] which was estimated to be 0.27(6). Unfortunately, size of the X-ray beam was larger than the size of the

twins and we were not able to perform an experiment to determine the twin sizes. On the other hand the fact that the crystal was racemic was further confirmed by absence of any detectable X-ray natural circular dichroism signal at the Fe *K*-edge in another piece of the same crystal. Note that XNCD signal at Fe *K*-edge in an enantiopure $RFe_3(BO_3)_4$ could be about 1% with respect to the edge jump [14].

XANES and XMCD spectra of $Ho_{0.5}Nd_{0.5}Fe_3(BO_3)_4$ crystals at the Fe *K*-edge for axial and orthoaxial configurations are shown in Fig. 3a. Two XANES spectra are quite different reflecting strong X-ray natural linear dichroism in this crystal extending over whole spectral range. XMCD spectra are nicely structured but their amplitude is about 10 times weaker than what was measured at the *K*-edge of Fe^{3+} ions in a single crystal of $Y_3Fe_5O_{12}$ ferrite [31]. The weakness of the XMCD signal even under applied field of 17 Tesla indicates that this field is much weaker than antiferromagnetic exchange interaction between Fe^{3+} spins. At best this field leads to a very small canting of the Fe^{3+} magnetic moment, *i.e.* $\ll 5$ deg. The spectral shape of XMCD spectra of $Ho_{0.5}Nd_{0.5}Fe_3(BO_3)_4$ crystal is also very different from the one measured in $Y_3Fe_5O_{12}$. If in the pre-edge region which is dominated by quadrupolar $1s \rightarrow 3d$ transitions a dispersive like shape is observed for both cases, the XMCD spectra of $Ho_{0.5}Nd_{0.5}Fe_3(BO_3)_4$ exhibit fine structure at photon energies corresponding to transitions into 4*p* states whereas no signal observed in $Y_3Fe_5O_{12}$. These fine structures are also strongly anisotropic as evidenced by XMCD spectra recorded for two crystal orientations and are reflecting anisotropy of the 4*p* density of states in the conduction band of the crystal.

XANES and XMCD spectra collected at the Ho and Nd $L_{3,2}$-edges for two crystal orientations are reproduced in Fig. 3b and 3c, respectively. The Ho and Nd XANES spectra were normalized to unity above the L_3- and to one half above the L_2-edge. These XANES spectra are dominated by the strong resonances, so-called "white lines", which correspond to transitions from core 2*p* states to the 5*d* states of the rare-earth ions. On a low-energy side of the white line at the L_3-edge one can observe a very weak feature which is associated with quadrupole transitions $2p \rightarrow 4f$. Note that similar feature is absent at the L_2-absorption edge of both Nd and Ho. One can also see a noticeable difference in intensity of the white lines reflecting anisotropy between the *c*-axis and *ab*-plane of the unoccupied electronic density of states of the 5*d* shell in both the Ho and Nd atoms. Note that anisotropy in the XANES spectra is more pronounced at the L_3-edge and nearly absent at the L_2-edge of Ho^{3+}, whereas the opposite is observed in the case of Nd^{3+} spectra. It seems to indicate that in the case of Ho and Nd there is an anisotropy in occupation of $5d_{3/2}$ and $5d_{5/2}$ subshells.

Dipolar selection rules make the magnetic signal at the rare-earth $L_{3,2}$-absorption edges sensitive to the spin polarization of the 5*d* level as a result of a 4*f*-5*d* exchange interaction [32]. In the case of Ho, we observed two resonance peaks which correspond to the quadrupole resonance (just below the Ho L_3-absorption edge) and the dipole resonance (just above the L_3-absorption edge) [33]. It is worth noting that it has been previously shown for a holmium foil at the Ho L_3-edge [34] that the positive peak at 8077.5 eV is mainly the electric dipolar (E1: $2p \rightarrow 5d$) contribution, whereas the negative peak at 8070 eV originates additively from both E2 (E2: $2p \rightarrow 4f$) and E1 ones. In turn, the Ho L_2-edge XMCD spectra consist of a main negative peak at the edge and a weaker positive peak at higher energy. Similarly to Ho^{3+} XMCD spectra, the spectral shape of the XMCD signals at the Nd $L_{3,2}$-edges in our crystals is similar to those measured in the $Nd_2Fe_{14}B$ [35] and $NdMnO_3$ [36]. It has been shown [37,38] that the first feature (minimum) in the XMCD spectrum at the L_3-absorption edge of Nd is due to $2p_{3/2} \rightarrow 4f_{5/2}$ quadrupole transitions, whereas the second one (main maximum) corresponds to dipole transitions $2p_{3/2} \rightarrow 5d_{3/2,5/2}$. The spectral shape of XMCD signal of the Nd L_2-absorption edge corresponding to dipole transitions $2p_{1/2} \rightarrow 5d_{3/2}$ is similar to Ho L_2-spectrum but of opposite sign. Surprisingly, XMCD signal at the $L_{3,2}$-edges of Ho does not show any significant anisotropy, whereas the XMCD anisotropy is strongly pronounced at the both L_3- and L_2-edges of Nd^{3+} ion.

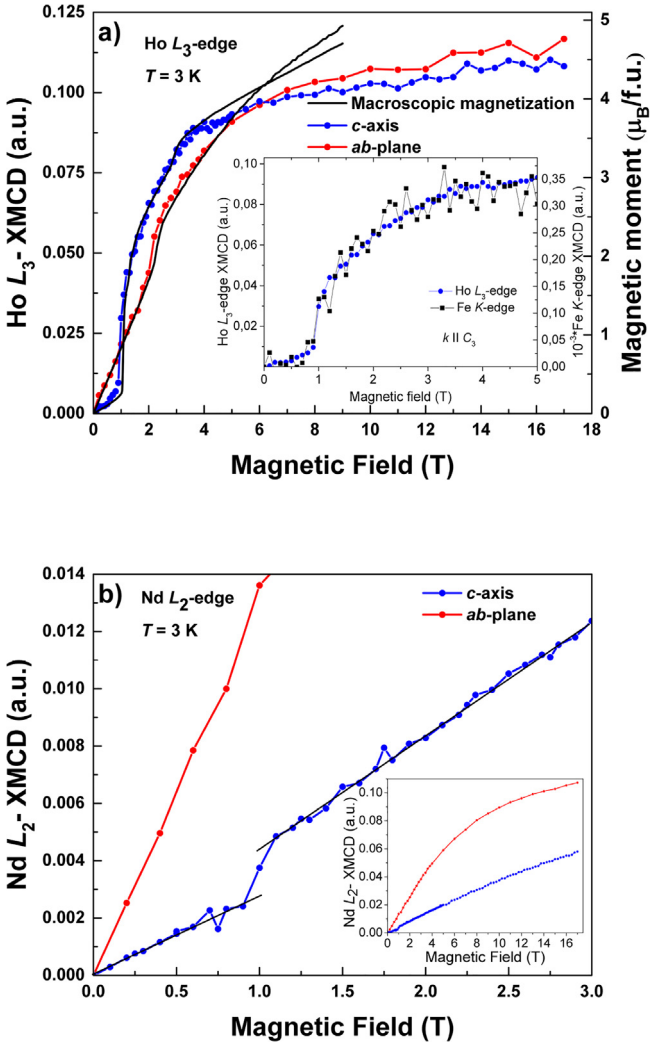

Fig. 4. (a) The element selective magnetization curves of $Ho_{0.5}Nd_{0.5}Fe_3(BO_3)_4$ as a function of applied field: a) Ho L_3-edge and bulk magnetization curves. The inset: the comparison of Ho L_3- and Fe *K*-edges XMCD magnetization curves for the applied field along the trigonal *c*-axis; b) Nd L_2-edge. The inset shows the linear dependence of the Nd L_2-edge XMCD magnetization on the applied field along the trigonal *c*-axis.

Unfortunately, we can not make use of magneto-optical sum rules to extract valuable information from XMCD spectra measured at the $L_{3,2}$-edges of rare-earth ions since the approximations used in their derivation are too crude [39]. The same applies to the *K*-edge of transition metals. However, the XMCD intensity at the $L_{3,2}$-edges of *RE* and the *K*-edge of transition metals was shown to be proportional to the atomic magnetization projected on the incident X-ray beam direction which is collinear with applied magnetic field. Therefore monitoring XMCD intensity as a function of applied magnetic field we record the so-called element selective magnetization curves.

The element selective magnetization curves of $Ho_{0.5}Nd_{0.5}Fe_3(BO_3)_4$ at the Fe *K*-, as well as at the Ho, Nd $L_{3,2}$-edges in comparison with macroscopic magnetization data are shown in Fig. 4. External magnetic field has a drastic and strongly anisotropic effect on the magnetic response of rare-earth and iron sublattices. The Ho magnetization measured with L_3-XMCD signal reveals a sharp increase at a critical field of $H_{sf}^{c} = 1$ T and a small step at ≈ 3 Tesla for a magnetic field applied along the trigonal *c*-axis (Fig. 4a). When magnetic field applied in the basal *ab*-plane, the jump in magnetization is weaker, smoother and is shifted towards higher fields ($H_{sf}^{ab} = 2.2$ T). These discontinuities in

magnetization curves are in perfect agreement with macroscopic measurements (see Fig. 2) and are experimental evidences of the spin-flop transitions in holmium atoms. In the field-induced spin-flop phase ($H < H_{sf}$) we observe first an increase of Ho magnetization due to rotation of magnetic moments but strikingly with no any sign of saturation both in the basal *ab*-plane and along the trigonal *c*-axis even above 10 Tesla field. It is worth noting that the Ho L_3-edge magnetization obtained from the XMCD data matches rather well the bulk magnetization measurements at low fields $H < 5$ T.

The Fe *K*-edge XMCD signal along the trigonal *c*-axis as a function of applied field is presented in the inset of Fig. 4a. The magnetic field induces a sharp jump in the iron magnetization at $H_{sf}^{c} = 1$ T exactly the same as that observed for the Ho magnetization curve. At the fields above H_{sf}^{c} the iron magnetization follows the holmium magnetization and this observation unambiguously shows that these two magnetic sublattices are strongly coupled. The Nd magnetization curves measured with XMCD at the Nd L_2-edge show completely different behavior (Fig. 4b). The applying magnetic field along the trigonal *c*-axis causes a visible jump in the magnetization at $H_{sf}^{c} = 1$ T. Observing this spin-flop transition at the exact same value of the field clearly indicates that all three sublattices are magnetically coupled. Note that for a pure $NdFe_3(BO_3)_4$ crystal the spin-flop transition is absent. However, a linear dependence of the magnetization above this transition is preserved. In contrast, for applied magnetic fields in the basal *ab*-plane the nonlinear behavior of the magnetization without any features is observed up to highest applied fields. For the applied field in the *ab*-plane the magnitude of the XMCD signal reaches ~0.11 at 17 T and is comparable with that found in a magnetically saturated state of Nd^{3+} ion in $Nd_2Fe_{14}B$ permanent magnet [40]. The Nd L_2-XMCD signal along the trigonal *c*-axis is observed to be nearly twice weaker even under 17 Tesla field (see inset of Fig. 4b) and this observation confirms the easy-plane anisotropy of Nd^{3+} ion in $Ho_{0.5}Nd_{0.5}Fe_3(BO_3)_4$. Moreover, the Nd magnetization is in turn affecting the magnetic behaviour of Ho and Fe sublattices as could be deduced from drastic difference of the critical fields of spin-flop transitions observed in $Ho_{0.5}Nd_{0.5}Fe_3(BO_3)_4$ crystal compared to the pure $HoFe_3(BO_3)_4$ crystal.

4. Conclusions

The Fe *K*-edge, Ho $L_{3,2}$-edge and Nd $L_{3,2}$-edge XMCD spectra have been measured at $T = 3$ K under magnetic fields of ± 17 T for the $Ho_{0.5}Nd_{0.5}Fe_3(BO_3)_4$ single crystal. Strong anisotropy of XMCD was found for Nd and Fe XMCD spectra, whereas the Ho ones appear to be similar for two orientations of the crystal along the trigonal *c*-axis and in the *ab*-plane. XMCD detected element selective magnetization curves have been also measured for two orientations of the crystal for all three magnetic sublattices. These results unambiguously show that in the $Ho_{0.5}Nd_{0.5}Fe_3(BO_3)_4$ there is a strong magnetic coupling between Nd^{3+}, Ho^{3+} and Fe^{3+} ions. It was found, that all three magnetic sublattices undergo a sharp spin-flop transition at $H_{sf}^{c} = 1$ T when magnetic field is applied along the trigonal *c*-axis, whereas Nd magnetization does not show a discontinuity in magnetization at $H_{sf}^{ab} = 2.2$ T as observed with Ho for magnetic field applied in the *ab*-plane. This result allows us to conclude that the spin-flop transitions observed in macroscopic magnetization curves and associated anomalies of electric polarization [21] are due to the Ho^{3+} magnetic moment reorientation. To get a more detailed insight into magnetoelectric coupling in this family of crystals, we plan to extend our measurements to enantiopure crystals.

Acknowledgements

The study was supported in part by the grants of the Russian Foundation for Basic Research (project Nos. 16-32-60049, 17-02-00826, 18-42-243007) and the Foundation for Assistance to Small Innovative Enterprises (FASIE, UMNIK program). The magnetic measurements were carried out in the Shared Facility Centre of P.N. Lebedev Physical Institute of RAS. We are grateful to Dr. Alexey Bosak for providing assistance of the structural experiments on the ID28 beamline. We are also grateful to Dr. Evgeniy Eremin from Kirensky Institute of Physics for providing the results of magnetic measurements and for useful discussions. The authors thank the ID12 beamline staffs for help during the XMCD experiment and also gratefully acknowledge the beamtime provision (proposal HC-1804) by the ESRF.

References

[1] A.K. Zvezdin, G.P. Vorob'ev, A.M. Kadomtseva, Yu.F. Popov, A.P. Pyatakov, L.N. Bezmaternykh, A.V. Kuvardin, E.A. Popova, J. Exp. Theor. Phys. Lett. 83 (11) (2006) 509–514.
[2] K.C. Liang, R.P. Chaudhury, B. Lorenz, Y.Y. Sun, L.N. Bezmaternykh, V.L. Temerov, C.W. Chu, Phys. Rev. B 83 (18) (2011) 180417 .
[3] A.K. Zvezdin, S.S. Krotov, A.M. Kadomtseva, G.P. Vorob'ev, Y.F. Popov, A.P. Pyatakov, E.A. Popova, J. Exp. Theor. Phys. Lett. 81 (6) (2005) 272–276.
[4] A.M. Kadomtseva, Y.F. Popov, G.P. Vorob'ev, A.A. Mukhin, V.Y. Ivanov, A.M. Kuz'menko, L.N. Bezmaternykh, J. Exp. Theor. Phys. Lett. 87 (1) (2008) 39–44.
[5] A.M. Kadomtseva, Y.F. Popov, G.P. Vorob'ev, A.P. Pyatakov, S.S. Krotov, K.I. Kamilov, L.N. Bezmaternykh, Low Temp. Phys. 36 (6) (2010) 511–521.
[6] A.M. Kadomtseva, G.P. Vorob'ev, Y.F. Popov, A.P. Pyatakov, A.A. Mukhin, V.Y. Ivanov, L.N. Bezmaternykh, J. Exp. Theor. Phys. 114 (5) (2012) 810–817.
[7] R.P. Chaudhury, B. Lorenz, Y.Y. Sun, L.N. Bezmaternykh, V.L. Temerov, C.W. Chu, J. Appl. Phys. 107 (9) (2010) 09D913.
[8] A.A. Mukhin, G.P. Vorob'ev, V.Y. Ivanov, A.M. Kadomtseva, A.S. Narizhnaya, A.M. Kuz'menko, I.A. Gudim, J. Exp. Theor. Phys. Lett. 93 (5) (2011) 275–281.
[9] A.A. Demidov, D.V. Volkov, Phys. Solid State 53 (5) (2011) 985–996.
[10] A.M. Kuzmenko, D. Szaller, Th. Kain, V. Dziom, L. Weymann, A. Shuvaev, A. Pimenov, A.A. Mukhin, V.Yu. Ivanov, I.A. Gudim, L.N. Bezmaternykh, A. Pimenov, Phys. Rev. Lett. 120 (2) (2018) 027203 .
[11] I.A. Gudim, A.A. Demidov, E.V. Eremin, D.K. Shukla, Phys. Solid State 60 (10) (2018) 1989–1998.
[12] R. Arun Kumar, (2012). J. Chem., 2013, Article ID 154862.
[13] Ch. Chen, T. Sasaki, R. Li, Yi Wu, Zh. Lin, Yu. Mori, Zh. Hu, J. Wang, G. Aka, M. Yoshimura, Yu. Kaneda, Nonlinear Optical Borate Crystals: Principals and Applications, Wiley-VCH Verlag & Co, KGaA, Weinheim, Germany, 2012.
[14] M. Platunov et al., unpublished results.
[15] T. Usui, Y. Tanaka, H. Nakajima, M. Taguchi, A. Chainani, M. Oura, S. Shin, N. Katayama, H. Sawa, Y. Wakabayashi, T. Kimura, Nat. Mater. 13 (2014) 611–618.
[16] A.M. Kuzmenko, A. Shuvaev, V. Dziom, A. Pimenov, M. Schiebl, A.A. Mukhin, A. Pimenov, Phys. Rev. B 89 (17) (2014) 174407 .
[17] J.C. Joubert, W.B. White, R. ROy, J. Appl. Crystallogr. 1 (5) (1968) 318–319.
[18] K.V. Frolov, I.S. Lyubutin, E.S. Smirnova, O.A. Alekseeva, I.A. Verin, V.V. Artemov, S.A. Kharlamova, L.N. Bezmaternykh, I.A. Gudim, J. Alloy. Compd. 671 (2016) 545–551.
[19] Y. Hinatsu, Y. Doi, K. Ito, M. Wakeshima, A. Alemi, J. Solid State Chem. 172 (2) (2003) 438–445.
[20] A.I. Begunov, A.A. Demidov, I.A. Gudim, E.V. Eremin, J. Exp. Theor. Phys. 117 (5) (2013) 862–874.
[21] R.P. Chaudhury, F. Yen, B. Lorenz, Y.Y. Sun, L.N. Bezmaternykh, V.L. Temerov, C.W. Chu, Phys. Rev. B 80 (10) (2009) 104424 .
[22] D.V. Volkov, A.A. Demidov, N.P. Kolmakova, J. Exp. Theor. Phys. 104 (2007) 897.
[23] A. Pankrats, G. Petrakovskii, A. Kartashev, E. Eremin, V. Temerov, J. Phys.: Condens. Matter 21 (2009) 436001 .
[24] J.E. Hamann-Borrero, S. Partzsch, S. Valencia, C. Mazzoli, J. Herrero-Martin, R. Feyerherm, E. Dudzik, C. Hess, A. Vasiliev, L. Bezmaternykh, B. Büchner, J. Geck, Phys. Rev. Lett. 109 (26) (2012) 267202 .
[25] V. Dyadkin, P. Pattison, V. Dmitriev, D. Chernyshov, J. Synchrotron Radiat. 23 (2016) 825–829.
[26] A. Rogalev, F. Wilhelm, J. Goulon, G. Goujon, Advanced Instrumentation for X-ray Magnetic Circular Dichroism, Magnetism and Synchrotron Radiation: Towards the Fourth Generation Light Sources, Springer International Publishing, 2013, pp. 289–314.
[27] J. Goulon, A. Rogalev, G. Goujon, C. Gauthier, E. Moguiline, A. Solé, P. Dressler, J. Synchrotron Radiat. 12 (1) (2005) 57–69.
[28] P. Fischer, V. Pomjakushin, D. Sheptyakov, L. Keller, M. Janoschek, B. Roessli, J. Schefer, G. Petrakovskii, L. Bezmaternikh, V. Temerov, J. Phys.: Condens. Matter 18 (34) (2006) 7975.
[29] C. Ritter, A. Vorotynov, A. Pankrats, G. Petrakovskii, V. Temerov, I. Gudim, R. Szymczak, J. Phys.: Condens. Matter. 20 (36) (2008) 365209 .
[30] H.D. Flack, Helv. Chim. Acta 86 (4) (2003) 905–921.
[31] A. Rogalev, J. Goulon, F. Wilhelm, C. Brouder, A. Yaresko, J.B. Youssef, M.V. Indenbom, J. Magn. Magn. Mater. 321 (23) (2009) 3945–3962.
[32] R.M. Galéra, Y. Joly, A. Rogalev, N. Binggeli, J. Phys.: Condens. Matter. 20 (39) (2008) 395217 .
[33] S. Nandi, A. Kreyssig, L. Tan, J.W. Kim, J.Q. Yan, J.C. Lang, A.I. Goldman, Phys. Rev. Lett. 100 (21) (2008) 217201 .
[34] L. Bouchenoire, A. Mirone, S.D. Brown, P. Strange, T. Wood, P. Thompson, J. Fernández-Rodríguez, New J. Phys. 11 (12) (2009) 123011 .
[35] J. Chaboy, F. Bartolomé, L.M. Garcıa, G. Cibin, Phys. Rev. B 57 (10) (1998) R5598.
[36] F. Bartolomé, J. Herrero-Albillos, L.M. Garcia, J. Bartolomé, N. Jaouen, A. Rogalev, J. Appl. Phys. 97 (10) (2005) 10A503.
[37] G. Kumar, J. Eckert, S. Roth, W. Löser, L. Schultz, S. Ram, Acta Mater. 51 (2003) 229.
[38] G. Kumar, O. Filip, W. Löser, L. Schultz, J. Eckert, Intermetallics 14 (2006) 47.
[39] H. Wende, Rep. Progr. Phys. 67 (12) (2004) 2105.
[40] A.P. Menushenkov, V.G. Ivanov, I.V. Shchetinin, D.G. Zhukov, V.P. Menushenkov, I.A. Rudnev, A.A. Ivanov, F. Wilhelm, A. Rogalev, A.G. Savchenko, J. Exp. Theor. Phys. Lett. 105 (1) (2017) 38–42.